Supplementary Information

Three-dimensional Hexagonal Fluorine-doped Tin Oxide Nanocone Arrays: A Superior Light Harvesting Electrode for High Performance Photoelectrochemical Water Splitting

Jinkai Li [a], Yongcai Qiu [a,c], Zhanhua Wei [a], Qingfeng Lin [b], Qianpeng Zhang [b], Keyou Yan [a], Haining Chen [a], Shuang Xiao [a], Zhiyong Fan [b] and Shihe Yang *[,a]

Table S1 Methods for preparing phosphorate buffer solution by using Na_2HPO_4 and NaH_2PO_4.

pH	0.2 mol/L Na_2HPO_4（ml）	0.2 mol/L NaH_2PO_4（ml）	pH	0.2 mol/L Na_2HPO_4（ml）	0.2 mol/L NaH_2PO_4（ml）
5.9	10.0	90.0	7.0	61.0	39.0
6.0	12.3	87.7	7.1	67.0	33.0
6.1	15.0	85.0	7.2	72.0	28.0
6.2	18.5	81.5	7.3	77.0	23.0
6.3	22.5	77.5	7.4	81.0	19.0
6.4	26.5	73.5	7.5	84.0	16.0
6.5	31.5	68.5	7.6	87.0	13.0
6.6	37.5	62.5	7.7	89.5	10.5
6.7	43.5	56.5	7.8	91.5	8.5
6.8	49.0	51.0	7.9	93.5	7.5
6.9	55.0	45.0	8.0	94.7	5.3

Supplementary Figures

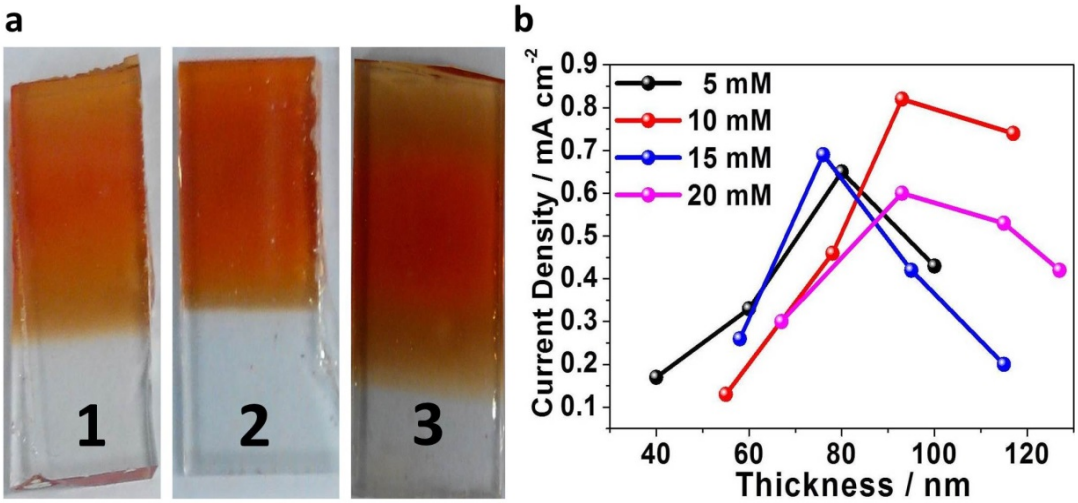

Figure S1 Influence of film thickness and precursor concentration. (a) Undoped-Fe_2O_3 thin film on planar FTO glass substrate with an increasing thickness from a to c; (b) Current density values of a certain precursor concentration with a certain thickness. We changed the Fe_2O_3 precursor concentration from 5 mM to 20 mM and at each concentration we prepared several samples with different thickness and tested the PEC performance. We found that 10mM precursor concentration with a film thickness of around 90nm could provide the highest current density at 1.23 V vs RHE. The film thickness was controlled by depositing time and the thickness was measured and estimated by AFM.

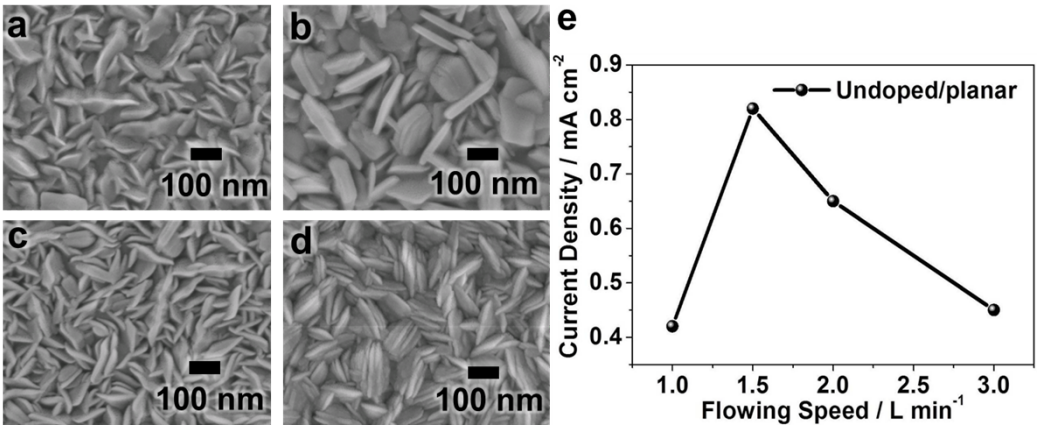

Figure S2 Influence of the carrier gas flowing speed. (a)-(d) show the different morphologies of Fe_2O_3 thin film when deposited with a carrier gas flowing speed of 1.0 L min^{-1}, 1.5 L min^{-1}, 2.0 L min^{-1}, 3.0 L min^{-1}, respectively. The corresponding photocurrent densities at 1.23 V vs RHE were collected in (e), which indicates the best flowing speed of 1.5 L min^{-1}.

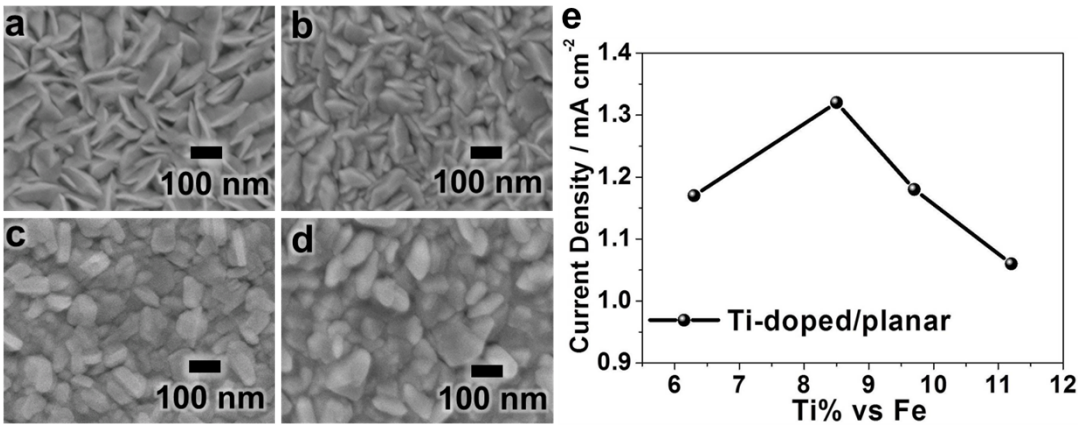

Figure S3 Influence of the Ti doping amount. (a)-(d) show the different morphologies of Fe_2O_3 thin film when doped with a Ti/Fe ratio of 6.3%, 8.5%, 9.7% and 11.2%, respectively, under a carrier gas flowing speed of 1.5 L min^{-1}. The corresponding photocurrent densities at 1.23 V vs RHE were collected in (e), which indicates the best Ti doping ratio of 8.5%.

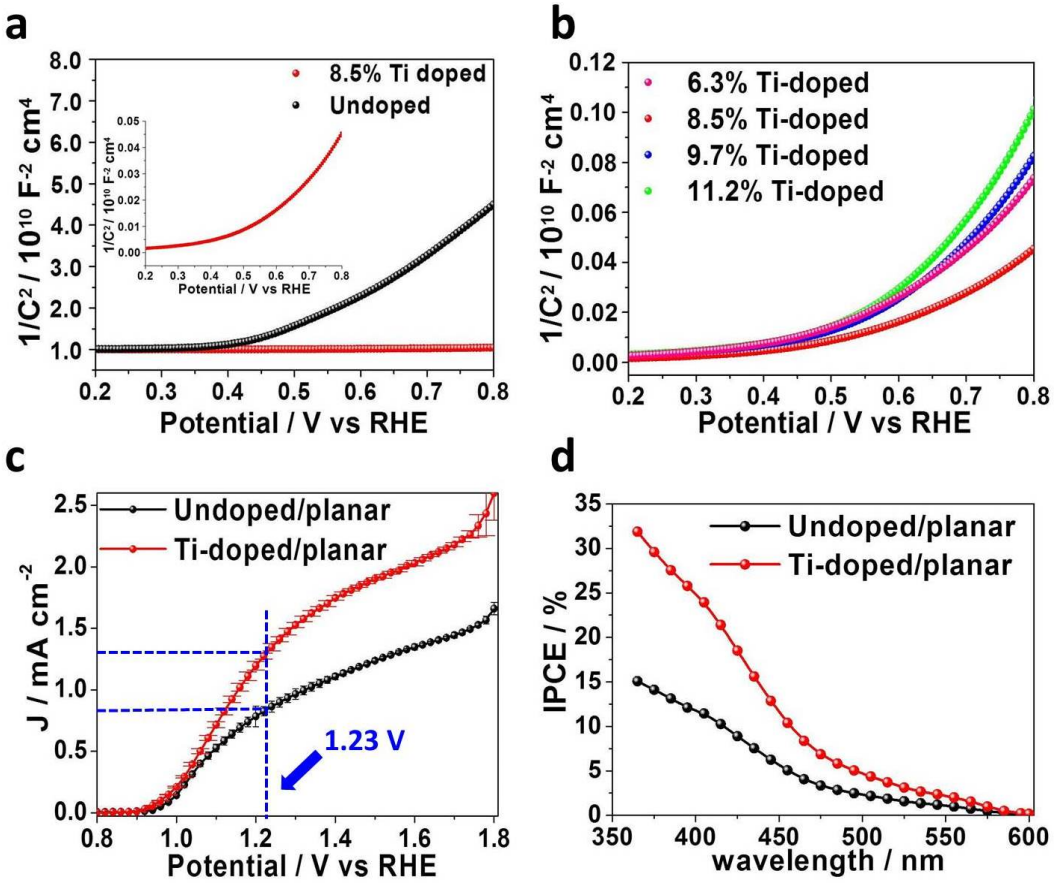

Figure S4 (a)-(b): Mott-Schottky plots of the films made of the undoped hematite and the 6.3%, 8.5%, 9.7%, 11.2% Ti-doped hematite thin film on planar FTO substrates. Capacitances were obtained from the electrochemical impedance at frequency of 1 kHz and an AC current of 10 mV with the three-electrode system aforementioned in the article in the dark. (a) indicates that the donor density in our doped hematite thin film (black curve) has been extremely enhanced compared with the undoped one (red curve). (b) illustrates the Mott-Schottky plots of different ratio Ti-doped hematite thin films, from which we could see that a doping amount of 8.5% by mole provided the largest donor density. (c)-(d): J-V curves and IPCE spectrums of the undoped and 8.5% Ti-doped sample on planar FTO glass, respectively, from which we could see that the PEC performance has been enhanced after Ti-doping. The error bars on each data point show the standard deviation of the present value during 10 repeated scans.

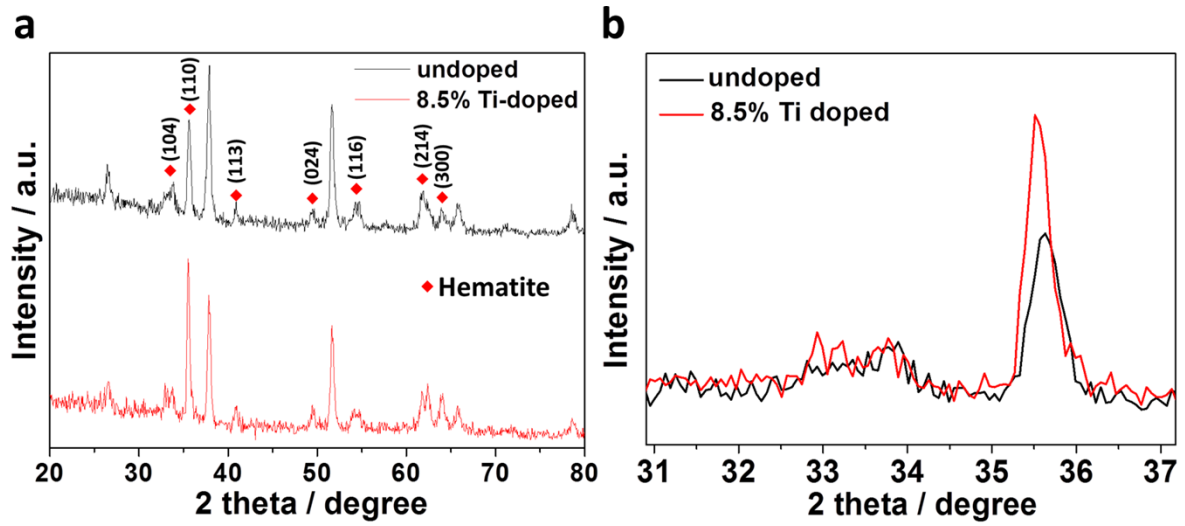

Figure S5 (a), XRD patterns of undoped and 8.5% Ti-doped hematite and (b), details of the peak information of (110) crystalline plane. We could observe that after doping with Ti element, the typical hematite peaks become stronger and there is an obvious shift of (110) peak, which means the Ti element has been successfully doped into the hematite crystal.

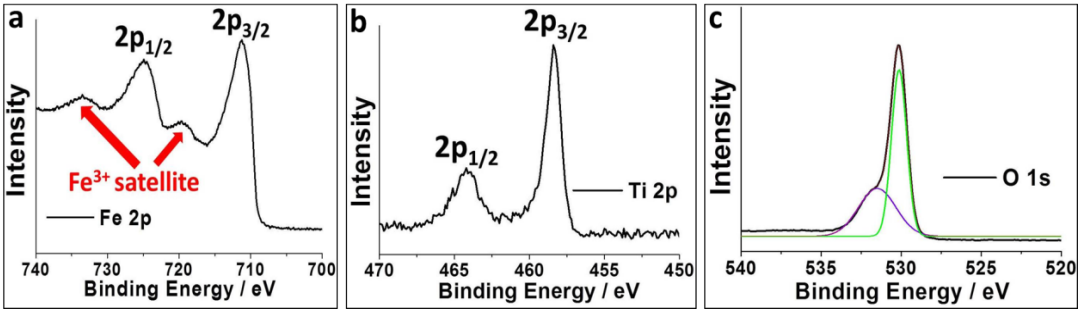

Figure S6 XPS analysis of Ti-doped Fe_2O_3. (a) - (c) show the XPS spectrum of Fe 2p, Ti 2p and O 1s core levels detected from the surface of samples after USP deposition, followed by annealing at 550°C. The binding energy of photoelectrons from Fe $2p_{1/2}$ and Fe $2p_{3/2}$ are about 724.6 eV and 710.9 eV, respectively, which arise from spin-orbit interaction and indicate the existence of iron elements in our sample. For Fe element, the satellite peaks are very important to identify the valence state. The spectra exhibits two special peaks at 719.2 eV and 733.1 eV, which could be identified as the satellite peaks of Fe(III). No shoulder peaks could be observed at around 715.0 eV which proves the non-existence of Fe(II). The binding energy for Ti $2p_{1/2}$ and Ti $2p_{3/2}$ could be observed at 463.9 eV and 458.1 eV, which are typical XPS peaks of Ti(IV). For O 1s spectrum, after Gaussian fitting, the binding energy at around 530.0 eV (green curve) could be assigned to the oxygen bound to Fe(III) and Ti(IV). Besides, a shoulder fitting peak at 531.8 eV (purple curve) could be seen in the spectrum, indicating the existence of oxygen vacancies.

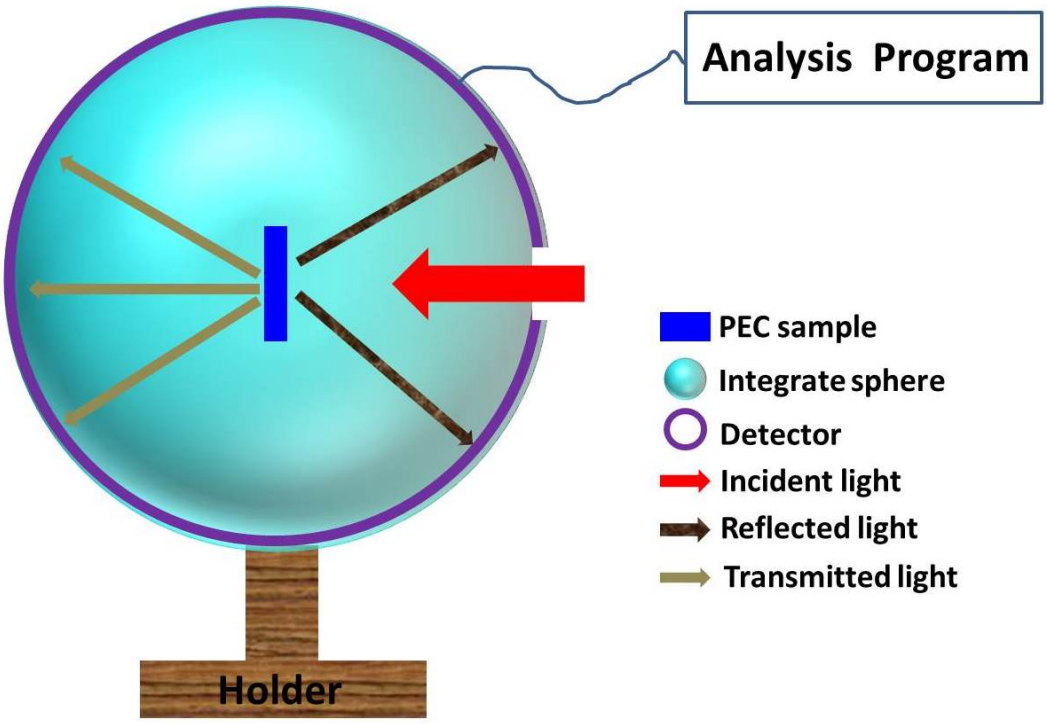

Figure S7 Self-made UV-Vis analysis system with an integrate sphere. The intensities of incident light (I), reflected light (R) and transmitted light (T) will be collected by computer and the absorption (A) of PEC sample could be calculated by the following equation: $A = 1 - \frac{R + T}{I}$.

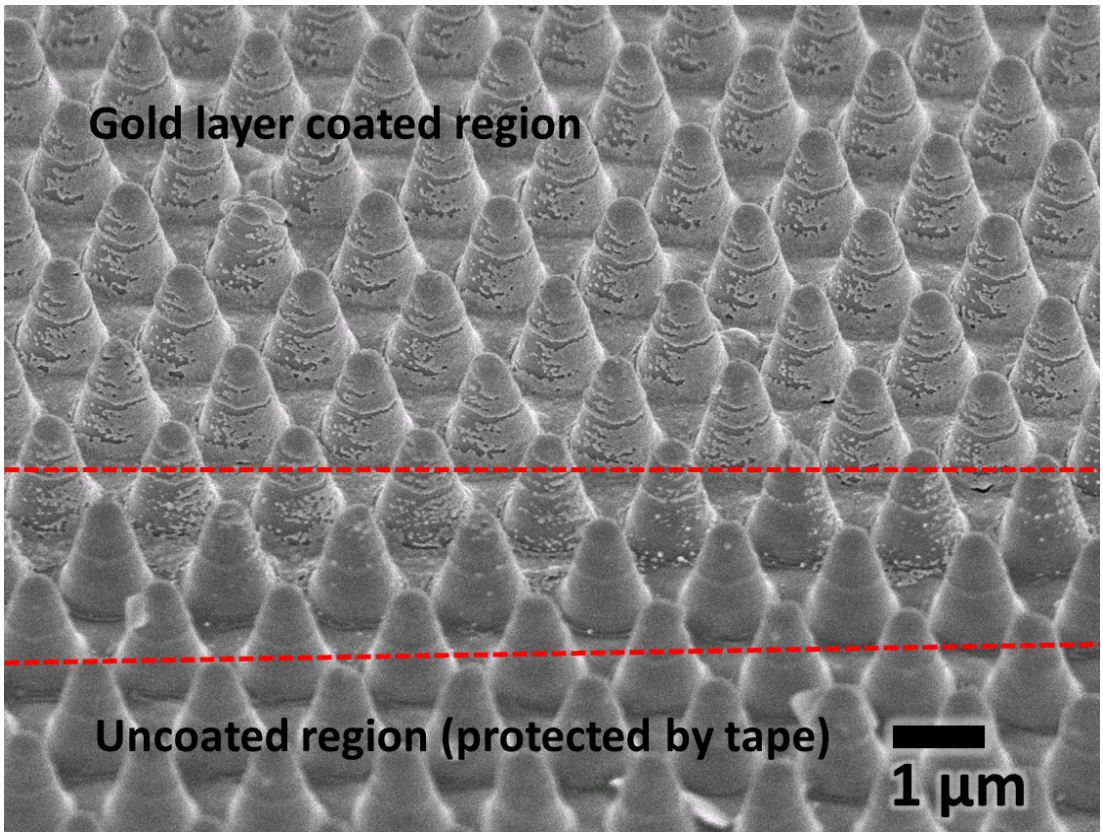

Figure S8 SEM image of gold-coated/uncoated 3D FTO nanocone array after treated with high temperature. The uncoated part was protected by tape when carrying out gold coating process. From this picture we could see that part of the gold layer will aggregate into gold nanoparticles under high temperature. The region between two red lines is the juncture of the coated and uncoated part.

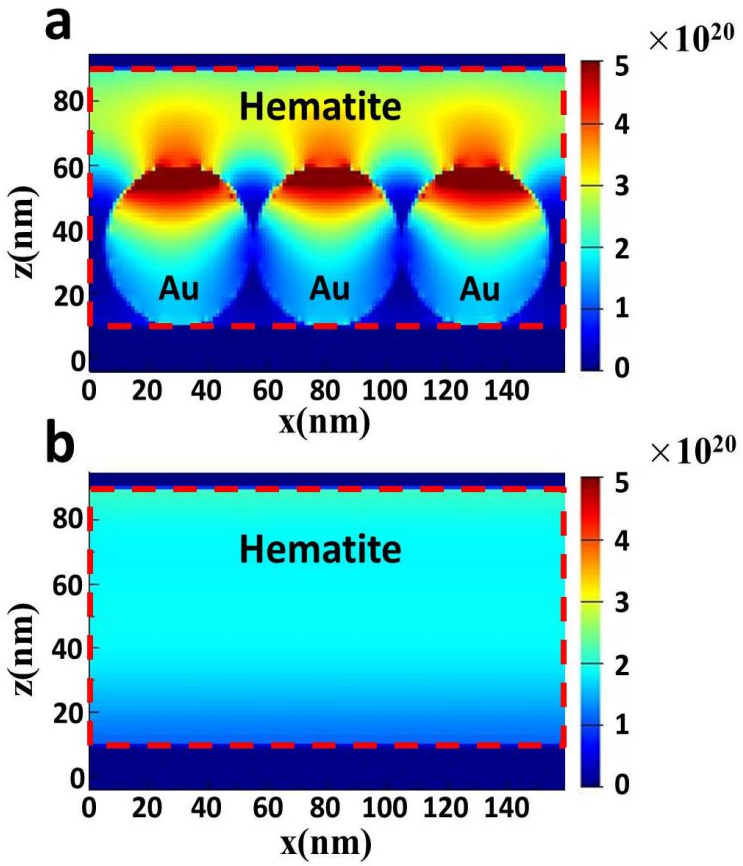

Figure S9 FDTD power absorption simulations of hematite active layer (a) with and (b) without aggregated gold nanoparticles at an incident wavelength of 500 nm. The color index at the right position of each figure reflects the absorption intensity at that point. The hematite layer region has been indicated by red dash rectangular. We could obviously see that the absorption intensity of hematite layer, especially at the upper 20 nm just above the gold nanoparticles, has been greatly improved due to the plasmonic effect provided by aggregated Au nanoparticles.

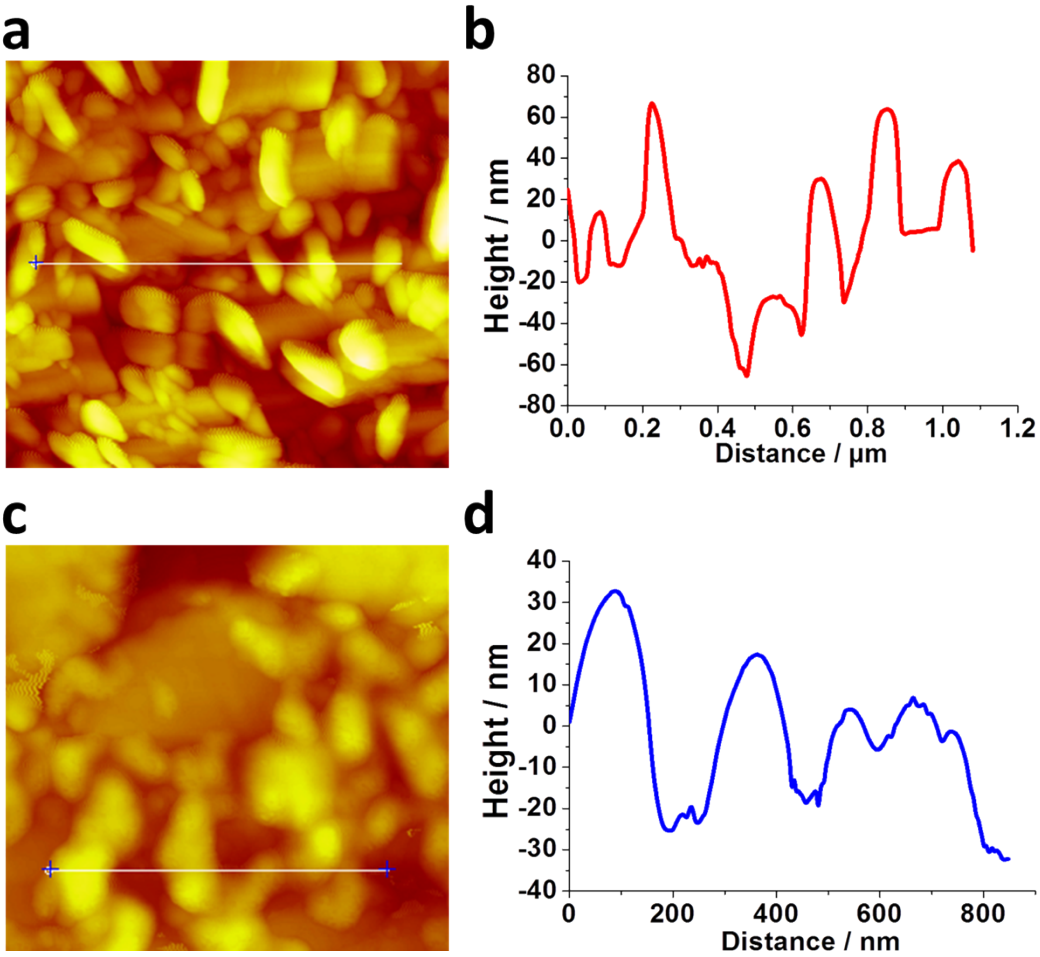

Figure S10 Surface AFM images of the Fe_2O_3 thin film (a) without Co-Pi catalyst and (c) with Co-Pi catalyst, from which we could see that after electrodepositing of Co-Pi catalyst, the surface of the film becomes smoother and thus it could help us to estimate the thickness of catalyst layer. (b) and (d) are the height spectrums along the white indicating line in (a) and (c), respectively.

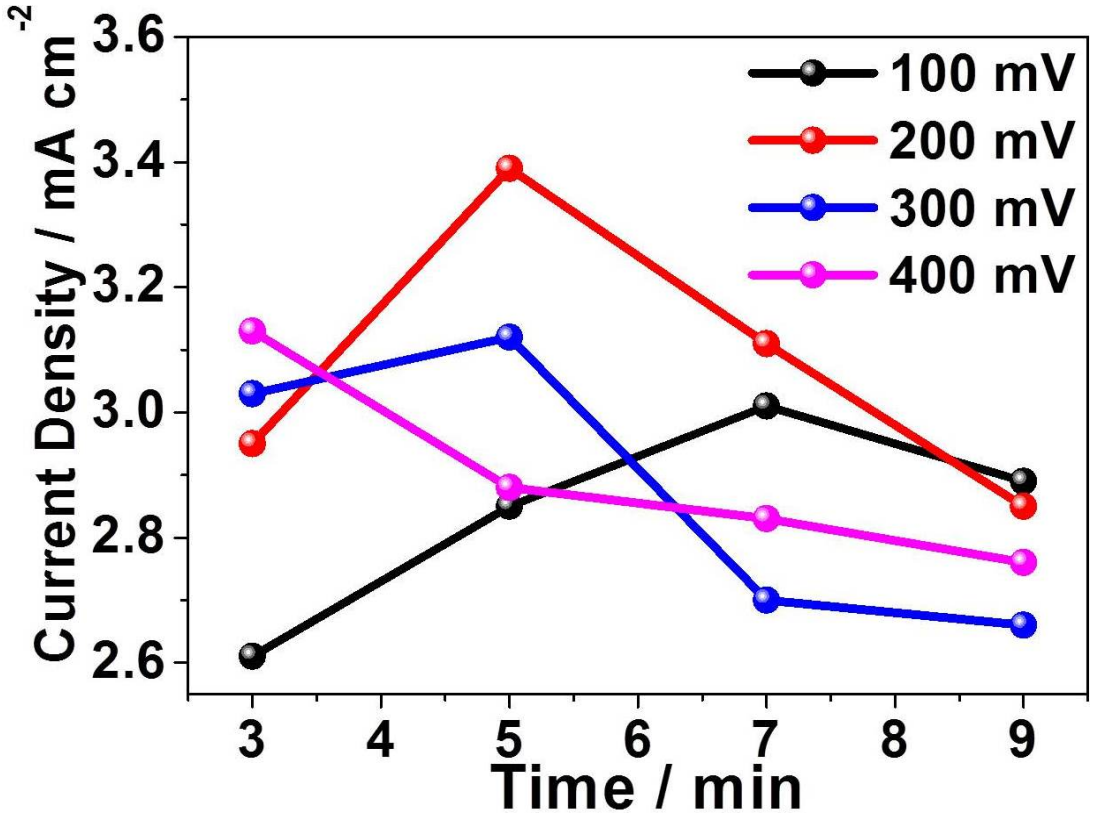

Figure S11 Influence of deposition method of Co-Pi catalyst. We changed the photo-assisted electrodepositing bias from 100 mV to 400 mV, and at each bias we changed the depositing time from 3 minutes to 9 minutes. We found that the Co-Pi catalyst deposited under a bias of 200 mV for 5 minutes could provide the highest current density at 1.23 V vs RHE. In addition, under different depositing conditions, the values of onset potential cathodic shift varied from 150 mV to 360 mV with no obvious regularity.

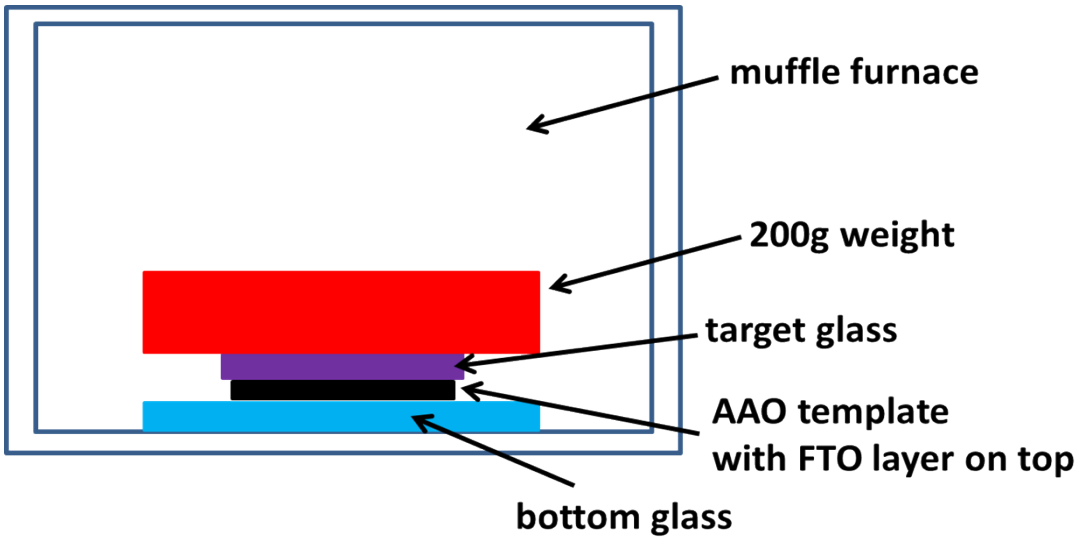

Figure S12 Schematic illustrating the 3D nanocone array pattern transfer from an AAO template to a glass substrate with FTO.